PERGAMON

International Journal of Heat and Mass Transfer 44 (2001) 1323–1342

International Journal of HEAT and MASS TRANSFER

www.elsevier.com/locate/ijhmt

Determination of the quench velocity and rewetting temperature of hot surfaces. Part I: analytical solution of the micro-scale hydrodynamic model

M. Ben David [a], Y. Zimmels [a,*], Y. Zvirin [b]

[a] *Department of Civil Engineering, Technion – Israel Institute of Technology, Haifa 32000, Israel*
[b] *Department of Mechanical Engineering, Technion – Israel Institute of Technology, Haifa 32000, Israel*

Received 10 June 1999; received in revised form 15 May 2000

Abstract

The hydrodynamic micro-scale model, developed previously, is used to solve the non-isothermal interface equation. The complex interface equation is simplified in a coordinate frame that moves with the three-phase contact line. This equation accounts for effects of evaporation, thermo-capillary and intermolecular forces. The new non-isothermal interface equation provides generalization of de Gennes' equation that applies to the isothermal case. The simplified third-order differential equation is solved numerically, and the effect of numerical parameters and selection of boundary conditions on solution convergence are established for a wide range of properties of solid–liquid pairs. In contrast to the smooth isothermal interfaces, non-isothermal interfaces are characterized by an undulating or wavy geometry. This behavior is a reflection of evaporation and mass transfer occurring across the interface, and unique capillary and thermocapillary effects that arise under non-isothermal conditions. A parametric study of the interface solution shows that increase of the capillary, C, and thermocapillary, $C\theta_0^2/F$ numbers produces steeper interface profiles, whereas the factor N, evaporation coefficient S, and the Hamaker constant $\bar{A}$, produce the reverse effect. Larger values of N, S and $\bar{A}$ result in higher undulation frequencies. These effects intensify and become dominant under rewetting conditions. The new interface equation provides an advanced tool for further studies of hydrodynamic mechanisms that govern the motion of thin liquid films on hot solid surfaces, that involve high temperature gradients and intense evaporation. This furnishes a hydrodynamic foundation for analysis of rewetting phenomena, and the definition of rewetting temperature and quench velocity, that are presented in a subsequent paper.

1. Introduction

The formulation of a non-isothermal, microscale hydrodynamic model of the three-phase contact zone near the quench front, which propagates during rewetting of hot surfaces, is given elsewhere [1], and summarized in Appendix A. In this process, a contact line is formed at the triple point on the solid, separating the liquid and vapor (see Fig. 12). The interaction between the three phases in this zone determines the velocity and affects the dynamics of the flow field behind the rewetting quench front.

The processes at and near the contact line are quite complex [2], involving several phenomena (hydrodynamics, thermodynamics, heat transfer, intermolecular forces, surface tension). Huh and Scriven [3] considered the case of simple fluid wedge and showed that the wedge profile leads to a logarithmic singularity in the viscous dissipation term. Body forces affect the film spreading on solid in a classical sense: gravity will greatly promote the spreading if the hydrostatic head is appreciable. In very small scales, where gravity is negligible, the solid–liquid attraction forces become dominant. Surface forces enter the description through the liquid–gas interface on which surface tension acts. Furthermore, if the contact line moves, and the no-slip condition is applied on the solid–liquid interface, then, as shown by Dussan and Davis [4]

* Corresponding author.

0017-9310/01/$ - see front matter
PII: S0017-9310(00)00181-2

Nomenclature

a	characteristic molecular size (m)
a_1, a_2, a_3	coefficients of velocity profile, Eq. (6) (dimensionless)
A	Hamaker constant (J)
$\bar{A}$	Hamaker constant, $A/6\pi\eta_l U_0 L^2\theta_0$ (dimensionless)
C	capillary number, $\eta_l U_0/\sigma\theta_0^3$ (dimensionless)
E	parameter, $\lambda_l\Delta T/\rho_l H_l L U_0\theta_0^2$ (dimensionless)
E_T	numerical tolerance (dimensionless)
f	denotes function
F	parameter, $\gamma\Delta T/\sigma$ (dimensionless)
$h(\xi), h(x,t), h$	liquid–vapor interface profile: function of ξ, of (x,t), and general notation (dimensionless)
H	film thickness (height of interface) (m)
H_l	heat of evaporation (kJ/kmol)
j_s	mass flux in stationary coordinate system of the solid (dimensionless)
j_{CL}	mass flux in moving coordinate system attached to the contact line (quench front) (dimensionless)
J	mass flux at the interface (kg/m^2 s)
K	empirical velocity coefficient for U_0 (m/s)
L	horizontal scaling length, a/θ_0^2 (m)
m	empirical power in velocity correlation for U_0 (dimensionless)
M	molecular weight (kg/kmol)
n	number of grid points (dimensionless)
$\boldsymbol{n}$	unit vector normal to the interface
N	parameter, $\left(L\theta_0\alpha\rho_v H_l^2/\lambda_l T_s^{3/2}\right)(M/2\pi R)^{1/2}$ (dimensionless)
p	total pressure, $p = p_{hyd} + \phi$ (dimensionless)
p_{hyd}	hydrostatic pressure (dimensionless)
P	total pressure (Pa)
q_1, q_2, q_3	boundary conditions at $\xi = 0$, Eq. (24) (dimensionless)
R	universal gas constant (J/kmol K)
R^*	parameter, Eq. (7) (dimensionless)
S	parameter, $(L/\sigma\rho_v\theta_0)(\lambda_l\Delta T/L\theta_0 H_l)^2$ (dimensionless)
t	time (dimensionless)
T	temperature (K or °C)
ΔT	characteristic temperature difference, $T_w - T_s$ (K)
$u(z)$	velocity component in ξ (or x) direction (dimensionless)
u^*	contact line (quench front) velocity (dimensionless)
U	velocity of interface (m/s)
U_{rew}	rewetting (quench front) velocity (m/s)
U_0	representative quench front velocity $K\theta_0^m$ (m/s)
$\boldsymbol{V}$	velocity
w_1, w_2	coefficients, Eq. (20) (dimensionless)
x, X	horizontal coordinate in stationary system, along the solid wall (dimensionless, m)
z, Z	vertical coordinate, normal to the solid wall (dimensionless, m)

Greek symbols

α	molecular accommodation factor (dimensionless)
γ	slope of linear $\sigma(T)$ correlation (N/mK)
ϕ	total effective potential of intermolecular forces acting on liquid molecule (dimensionless)
η	dynamic viscosity (kg/m s)
λ	thermal conductivity (W/m K)
θ	contact angle (rad)
θ_0	reference contact angle (rad)
Θ	temperature (dimensionless)
ρ	density (kg/m^3)
σ	surface tension (N/m)
τ	time (s)
ξ	coordinate (in x-direction) in a moving frame of reference attached to the quench front, Eq. (1) (dimensionless)
$\Delta\xi$	grid size (dimensionless)

Subscripts

c	critical
l	liquid
s	saturation
v	vapor
w	wall (solid)
ξ	differentiation with respect to ξ

Superscript

I	interface (at $z = h$)

there is a force singularity at the contact line. The implication is that on the continuum level there is an effective slip of the liquid on the wall. In the two-dimensional case, where the liquid–vapor interface is located at $z = h(x,t)$, the interface slope, h_x, at the contact line, satisfies the condition $h_x(x,t) = -\tan\theta$, where θ is the contact angle.

If the interface moves with velocity U, then one may specify $\theta = f(U)$, which determines the mobility of the

contact line as discussed by Dussan [2] based on experimental observations in isothermal situations. Tanner [5] studied spreading (wetting) of droplets on a solid surface (without heat transfer). He considered viscous and capillary forces only and used lubrication theory to describe the behavior of the bulk fluid away from the contact line. He found empirical power laws for the droplet radius as a function of time, t, for large t: $r \sim t^{1/7}$ in the two-dimensional case and $r \sim t^{1/10}$ in the axisymmetric case. Lopez et al. [6] took a similar approach, but ignored capillarity, and included gravity or long-range molecular forces near the contact line. They found different power laws for the spreading rate of the contact line.

Another approach to spreading is that of de Gennes [7] who examined the small-scale physics of contact lines. His model includes long-range van der Waals repulsion, and predicts a rather large droplet, that possesses no contact line, but instead smoothly blends into a precursor film, which extends forward from the main bulk, far along the wall. This approach leads to useful information on the functional form of $U = f(\theta)$. Greenspan [8] considered a local slip near the contact line. In his model, the capillary and viscous forces are included, with the assumption of linear f. He used lubrication theory for flat droplets, and obtained an evolutionary system, giving the history of the interface form. Ehrhard and Davis [9] generalized Greenspan's approach, replacing the angle-versus-speed function by $U = K\theta_0^m$, where K is an empirical coefficient and the power m is called mobility exponent. Greenspan assumed $m = 1$, while they took $m = 3$, as suggested by Hoffman [10] and Tanner [5] using data on contact-line dynamics.

De Gennes et al. [11], discussed the local slopes $\theta(x)$ (interface profile), and the dominant physical cut-off for the line singularity. They showed that the slippage process does exist, but it is only relevant for a very small film thickness, where the whole continuum description breaks down. They concentrated on a situation of partial wetting, where four special regions around the contact line are distinguished: molecular, proximal, central and distal. The molecular region cannot be described by continuum theory. The proximal region is controlled by long-range forces, the central is controlled by shear flow plus capillarity and the distal region is controlled by shear flow plus gravitational forces. De Gennes [7] simplified the problem analysis considerably by attaching the reference coordinate frame to the triple line, so as to obtain a quasi-steady representation. The liquid–gas interface equation developed in his model incorporates the effects of capillarity, long-range forces (described by the Hamaker constant) and slow Poiseuille flows. He restricted his attention to situations of small slopes, i.e. $h_x \ll 1$. This allows the use of a linearized form for the capillary pressure, a lubrication approximation for the flow and a simple description of the van der Waals forces.

Ben David et al. [1] propose to extend the de Gennes approach so as to cover cases of non-uniform temperature and evaporation at the interface. A non-isothermal micro-scale model of the three phase (solid–liquid–vapor) contact zone is formulated in the context of rewetting phenomena. The model incorporates hydrodynamics, heat transfer, interfacial phenomena and intermolecular long-range forces, in a two-dimensional proximal region of the order of 1000 Å (100 nm) in width, and 100 Å (10 nm) in thickness. The model comprises scaled mass, momentum and energy balances, and their corresponding scaled boundary conditions. The small contact angles which are characteristic of rewetting situations facilitate the use of the lubrication approximation, and the dynamics of the liquid and gas phases is decoupled by applying the one-sided simplification. Thermo-capillary, conduction/evaporation and solid–liquid intermolecular attraction effects are expressed by appropriate dimensionless numbers. The present work includes the derivation of the interface equation, emerging from this model, its solution and a parametric study of the film thickness behavior.

2. Theory: derivation of the liquid–vapor interface equation

The model developed by Ben David et al. [1] for the proximal region near the three-phase contact line, comprises a system of partial scaled differential equations and boundary conditions, describing the hydrodynamics and heat transfer in this region. A summary of the balance equations, boundary conditions and main assumptions is presented in Appendix A. The system was derived by linearization through the lubrication approximation, and several other simplification procedures, e.g., the one-sided approach. In the present work, an analytical solution of this system is obtained, which leads to the derivation of an equation for the liquid–vapor interface, $h(x, t)$. Solving this equation for h enables determination of the three-phase contact zone where rewetting may occur. The flow and temperature fields, given in terms of $h(x, t)$, can then be written explicitly.

Appendix B includes a formal derivation of the complete interface equation. However, this equation is excessively complicated due to the transient treatment of the problem, as reported by de Gennes [7]. Therefore, an additional simplification of the linearized system of equations is suggested, in order to derive a more amenable interface equation, based on and extending his hydrodynamic approach. The interface equation for $h(x, t)$ is derived from the conservation equations and boundary condition balances developed by Ben David et al. [1]. The parameters here are dimensionless, according to the definitions, scaling, and notation introduced there (see Appendix A and the nomenclature).

De Gennes [7] showed that working with a coordinate frame attached to the moving contact line, greatly simplifies the hydrodynamic treatment of the problem. In rewetting situations, the liquid front moves at an almost constant velocity, and hence, a quasi-steady description of the interface profile is valid, cf., Olek et al. [12,13]. Therefore, using the contact line dimensionless velocity, u^*, defined later, in Eq. (8), the following transformation of coordinates is applied:

$$\xi = x - u^* t. \tag{1}$$

In this way $h = h(\xi)$ does not depend on the time, t, and the problem description is quasi-stationary. The temperature field, $\Theta(\xi, z)$, is obtained in terms of the interface profile h (unknown at this stage), by solving the energy Eq. (A.16) with the boundary conditions (A.17) and (A.21)

$$\Theta(\xi, z) = \frac{1 + N(h - z)}{1 + Nh}, \quad 0 \leqslant \xi \leqslant 1. \tag{2}$$

Note that according to the definitions, derivations and scaling, $0 \leqslant \xi \leqslant 1$ at the quasi-steady state that follows from Eq. (1). This corresponds to a dimensional range of 1000 Å (100 nm).

The temperature Θ^{I}, at the interface $z = h(\xi)$, takes the following form:

$$\Theta^{\mathrm{I}} = \frac{1}{1 + Nh}. \tag{3}$$

Two limiting cases may be distinguished in Eq. (3) as follows:

$$N \to 0 : \Theta^{\mathrm{I}} \to 1, \tag{4}$$

$$N \to \infty : \Theta^{\mathrm{I}} \to 0. \tag{5}$$

Thus, in both limits the temperature along the liquid–vapor interface tends to an a priori known constant. The case $N \to 0$ represents perfect conduction, where the temperature is uniform across the film, equal to that of the solid, see Eq. (2). In the second case, $N \to \infty$, the interface temperature becomes equal to the saturation temperature. After the interface equation is solved (in the following) to find $h(\xi)$, the temperature distribution $\Theta(\xi, z)$ can be determined explicitly.

De Gennes [7] suggested an elegant approach to analyze the dynamics of the three-phase contact line. His approach, which is limited to the isothermal case, is modified and extended here to treat non-isothermal conditions characterizing rewetting situations. The main assumption is that the film considered is very thin and flat, so that a parabolic velocity profile can be postulated

$$u(z) = a_1 z^2 + a_2 z + a_3, \tag{6}$$

where the coefficients a_1, a_2 and a_3 (which depend on ξ and t through h) are calculated by the boundary conditions. The no-slip condition at the wall, Eq. (A.17), yields $a_3 = 0$. Introducing the last expression and that for the temperature, Eq. (2), into the boundary condition at the interface $z = h$, as defined by Eq. (A.20), the following relation between a_1 and a_2 is obtained:

$$2a_1 h + a_2 = \frac{Nh_\xi}{\left(\frac{C0_0^2}{F}\right)(1 + Nh)^2} \equiv R^*. \tag{7}$$

A second relation between a_1 and a_2 is obtained by calculating the average dimensionless velocity, u^* (which is considered to be the velocity of the contact line, or quench front)

$$u^* = \frac{1}{h}\int_0^h (a_1 z^2 + a_2 z)\,\mathrm{d}z = \left[2a_1 h^2 + 3a_2 h\right]/6. \tag{8}$$

Solving Eqs. (7) and (8) for a_1 and a_2 gives

$$a_1 = -\frac{3u^*}{2h^2} + \frac{3R^*}{4h}, \quad a_2 = \frac{3u^*}{h} - \frac{R^*}{2}. \tag{9}$$

Introducing the second derivative of the velocity function, Eq. (6), into the momentum equation (force balance) in the horizontal direction, Eq. (A.14), gives

$$u_{zz} = 2a_1 = p_\xi. \tag{10}$$

By substituting the expression for a_1, Eq. (9), the following expression for the average velocity, u^*, is obtained:

$$u^* = -\frac{1}{3}\left[p_\xi - \frac{3R^*}{2h}\right]h^2. \tag{11}$$

The horizontal mass flux (in the coordinate frame of the solid), j_{s}, is given by multiplying the average velocity, u^*, by the layer thickness, h

$$j_{\mathrm{s}} = -\frac{1}{3}h^3 p_\xi + \frac{1}{2}R^* h^2. \tag{12}$$

In the frame of the moving contact line (CL), the flux j_{s} becomes

$$j_{\mathrm{CL}} = j_{\mathrm{s}} - u^* h. \tag{13}$$

For steady-state solutions, where no film exists far ahead of the contact line, j_{CL} must vanish. This leads to the following equation of the liquid–vapor interface:

$$-\frac{1}{3}h^2 p_\xi + \frac{1}{2}R^* h - u^* = 0. \tag{14}$$

The pressure distribution in the film can be obtained by combining the definition of the generalized pressure and the normal stress balance, Eqs. (A.11) and (A.19). This gives the following expression [7]:

$$\begin{aligned} p(\xi, z) &= p_{\mathrm{hyd}} + \phi \\ &= \frac{1}{C}\left[-h_{\xi\xi}(1 - F\Theta^{\mathrm{I}}) + Sj^2\right] - \frac{\bar{A}}{h^3} + \frac{\bar{A}}{z^3}. \end{aligned} \tag{15}$$

Differentiation of Eq. (15) with respect to ξ, substitution of the explicit expressions for j, Eq. (A.18), and

for Θ^{I} and R^*, Eqs. (3) and (7), and introduction into Eq. (14) yield a third-order non-linear ordinary differential equation for $h(\xi)$

$$h_{\xi\xi\xi}\left[1-\frac{F}{1+Nh}\right]+h_{\xi\xi}h_{\xi}\frac{FN}{(1+Nh)^2}+h_{\xi}\left[\frac{2SN^3}{(1+Nh)^3}-\frac{3C\bar{A}}{h^4}+\frac{3NF\theta_0^2}{2h(1+Nh)^2}\right]+\frac{3Cu^*}{h^2}=0, \tag{16}$$

where F, N, S, C, $\bar{A}$ and $NF\theta_0^2$ are dimensionless groups (their definitions appear in the nomenclature).

In order to get a better insight concerning the expected behavior of the solution of Eq. (16), the simpler isothermal case is considered first. In this case, $\Delta T = T_{\mathrm{w}} - T_{\mathrm{s}} = 0$, and hence,

$$F=0, \quad S=0, \quad C/F\to\infty. \tag{17}$$

Introducing these values into Eq. (16) yields

$$\sigma\theta_0^3 h_{\xi\xi\xi} - 3\eta_{\mathrm{l}}U_0\bar{A}h_{\xi}/h^4 + 3\eta_{\mathrm{l}}U_0u^*/h^2 = 0 \tag{18a}$$

and the dimensional form of this equation is obtained as

$$\sigma H_{XXX} - \frac{A}{2\pi}\frac{H_X}{H^4} + \frac{3\eta_{\mathrm{l}}u^*U_0}{H^2} = 0. \tag{18b}$$

Eq. (18b) was derived by de Gennes [7], for the isothermal, non-volatile case. Thus, the interface Eq. (16), developed in the present work, is an extension of de Gennes, where the effects of temperature gradients, evaporation and thermo-capillarity are included. The terms in Eqs. (18a) or (18b) express the capillary effect, the long-range forces due to the solid–liquid interaction and the viscous effect of the flow.

Eq. (16) of the liquid–vapor interface also includes the effect of temperature gradients along the interface. All the terms that contain different powers of $1/(1+Nh)$, e.g., the temperature Θ^{I} as per Eq. (3), are due to this gradient. For convenience, the seven terms of Eq. (16) (five of them are between parentheses) are identified by numbering them from left to right. Terms 2, 3, 4 and 6 are associated with the interface temperature, Θ^{I}. Terms 2, 3, 5, 6 and 7 include either F or C. The former one expresses the change in surface tension with temperature, and the latter is the capillary number, which is the ratio of the dissipative effects of the contact line velocity, and the variations of the mean surface tension.

From the definitions of C and F, it follows that their ratio

$$\frac{C}{F}=\frac{\eta_{\mathrm{l}}U_0}{\gamma\Delta T\theta_0^3} \tag{19}$$

is proportional to the thermo-capillary number. This is a consequence of the tangent shear stress boundary condition (A.20). Terms No. 2, 3, and 6 of Eq. (16) express the contribution of the thermo-capillarity effect. When the wall temperature increases, C/F decreases, and thus the effect of the tangential forces, which pull the liquid back against its tendency to spread on the solid surface, becomes more dominant. As the distance from the contact line increases, h increases, the interface temperature, being equal to $1/(1+Nh)$ decreases, and hence the surface tension there is expected to be higher than its value close to the contact line. High values of C/F may be associated with high viscosity liquids. In this case, the thermo-capillarity effect is expected to be negligible.

The fourth term of Eq. (16) includes the dimensionless number, S, which stands for the effect of evaporation at the interface and its associated recoil effect. This effect is described and explained in the sequel. At elevated levels of the wall temperature, the values of S are expected to be relatively large. In this case, the fourth term becomes dominant and the liquid–vapor interface is expected to be pressed towards the solid. Large values of ΔT may lead to significant perturbations of the liquid–vapor interface, but at the same time, higher temperature levels also cause the film to be flatter. This increases the solid–liquid attraction forces (term 5 in Eq. (16)) which act to relax the interface perturbations. These qualitative observations have been verified by specific solutions of the interface equation which are discussed quantitatively in the next section.

3. Solution of the liquid–vapor interface equation

3.1. Interface equation and boundary conditions

Eq. (16) is a non-linear ordinary differential equation of the third-order. It can be converted to a system of three ordinary first-order differential equations as follows:

$$\begin{aligned}
h_1(\xi) &= h(\xi),\\
\frac{\partial h_1(\xi)}{\partial\xi} &= h_2(\xi),\\
\frac{\partial h_2(\xi)}{\partial\xi} &= h_3(\xi),\\
\frac{\partial h_3(\xi)}{\partial\xi} &= \frac{3Cu^*}{w_1[h_1(\xi)]^2}+\frac{3FN\theta_0^2h_2(\xi)}{2w_1w_2^2h_1(\xi)}-\frac{3C\bar{A}h_2(\xi)}{w_1[h_1(\xi)]^4}\\
&\quad+\frac{FNh_2(\xi)h_3(\xi)}{w_1w_2^2}+\frac{2SN^3h_2(\xi)}{w_1w_2^3},
\end{aligned} \tag{20}$$

where w_1 and w_2 are defined by:

$$w_1=\frac{F}{1+Nh_1(\xi)}-1 \tag{21a}$$

$$w_2=1+Nh_1(\xi). \tag{21b}$$

In order to solve the third-order interface equation, or alternatively, the three-equation system (20), it is

necessary to define three boundary conditions. Due to the complexity of the three-phase contact zone, it is impossible to define them directly. For example, at $\xi = 0$, the variable h does not vanish and it must conform with molecular dimensions, e.g., of the order of a few Angstroms. At present, it is unknown what should be the appropriate height, $h(\xi = 0)$, and hence its value may only be guessed, or rather imposed on the system. The validity of the guess can then be tested once the solution, which relies on it, has been formulated. Using the conventional approach, the second boundary condition involves the derivative $h_\xi(\xi = 0)$. The third boundary condition is defined at $h(\xi = 1)$, e.g., the value of layer thickness at the other end of the film range studied. Successive trials of different combinations of these boundary conditions did not always produce a realistic solution for $h(\xi)$. Therefore, it was necessary to adopt a different approach, where all three boundary conditions are assigned at $\xi = 0$, in the form of "initial value" problem: h, h_ξ and $h_{\xi\xi}$ at $\xi = 0$, or using the notation of Eq. (20), h_1, h_2 and h_3 at $\xi = 0$.

The system of Eq. (20) was solved by a solver taken from the IMSL (1986) (International Mathematics Statistics Library). This solver consists of a subroutine named IVPRK, which uses a finite differences algorithm, based on the Runga–Kutta–Verner fifth/six orders method. This subroutine was found to be convenient because of its flexibility for changing the input parameters. For example, the discretization of the region $0 \leqslant \xi \leqslant 1$ in the form of a grid can be controlled so that a satisfactory shape of the interface profile is obtained. The number of allowed grid points is 500, which means that each step is of the order of a few Angstroms. The relative error may also be controlled by the user. To this end, the effect of changes in grid intervals, on the output relative errors, were tested until a satisfactory degree of solution accuracy has been achieved. In order to characterize a suitable combination of boundary conditions, a solution of the liquid–vapor interface, $h_1(\xi)$, and its derivatives, $h_2(\xi)$, $h_3(\xi)$, was worked out.

In the following, a parametric investigation of the way and extent in which boundary conditions affect the solution behavior is provided. This is done in order to determine their appropriate form, which leads to realistic solutions for different materials and different rewetting situations. Furthermore, as a preliminary step, the solution sensitivity to variation of the numerical parameters was examined. Numerical parameters were tested and selected separately for each specific solid–liquid system. The test procedure includes the following steps:

(a) Input of data of thermo-physical properties of the liquid at saturation temperature, T_s, and atmospheric pressure.

(b) Calculation of the dimensionless numbers that appear in Eq. (20) N, S, F, C, C/F and $\bar{A}$.

(c) Initially, the wall temperature was set at $T_w \cong 260°C$, as an estimate for the rewetting temperature of water on stainless steel. In this case, $\Delta T = T_w - T_s \cong 160°C$.

(d) In testing the effects of the numerical parameters, $h_1(\xi), h_2(\xi)$, and $h_3(\xi)$ were evaluated at $\xi = 0$, using the same scaling procedure that led to the derivation of Eq. (16). The following values were selected as a consequence of the choice of boundary conditions (see Section 3.3):

$$h_1 = 0.25, \quad h_2 = 1, \quad h_3 = 1 \quad \text{at} \quad \xi = 0. \tag{22}$$

For water on the stainless steel, the dimensional equivalents of these boundary conditions are O(1 nm), O(10^{-2} rad) and O(10^{-3} rad/nm), respectively.

(e) Once the system of Eq. (20) is defined by the values of its dimensionless numbers, the parametric investigation of the boundary conditions may be performed. At $\xi = 0$, there are three boundary conditions that should be tested. The procedure is to let one of them vary, while keeping the other two fixed, so that its isolated effect on the equation solution can be examined.

The following two Sections 3.2 and 3.3 include results of investigations and tests of the numerical parameters and boundary conditions. For water on stainless steel, these were performed with reference values of the dimensionless parameters in Eq. (16) given by

$$\begin{aligned} &u^* \cong 1, \quad \frac{C\theta_0^2}{F} = 2.8 \times 10^{-3}, \\ &N = 6.5 \times 10^{-3}, \quad C = 4.59, \quad \bar{A} = 0.2128, \\ &S = 164.5. \end{aligned} \tag{23a}$$

For helium on stainless steel, the corresponding reference values are

$$\begin{aligned} &u* \cong 1, \quad \frac{C\theta_0^2}{F} = 0.189, \quad N = 0.54, \\ &C = 1254, \quad \bar{A} = 7.8 \times 10^{-4}, \quad S = 867. \end{aligned} \tag{23b}$$

These numbers were evaluated by using the data specified in Table 1.

3.2. Testing of the numerical parameters

In order to ensure convergence, the effect of the grid size, $\Delta\xi_i$, and the tolerance (relative error), E_T, on the solution, $h(\xi)$, was investigated. The parameters tested, $\Delta\xi_i$ and E_T, are constrained by requirements of the subroutine used. The maximum number of grid points allowed within the interval $0 \leqslant \xi \leqslant 1$ is 500. The tolerance, E_T, is also constrained by a lower bound of 10^{-5}. These constraints were found to be adequate for solution of Eq. (20). The independent variable, ξ, varies between zero and one (corresponding to a dimensional

Table 1
Thermo-physical properties of various fluids

	Fluid properties at saturation conditions	Helium (He)	Water (H_2O)
p	Pressure (kPa)	103	103
T_s	Saturation temperature (°C)	−268.9	100
ρ_l	Liquid density (kg/m^3)	125	960
ρ_v	Vapor density (kg/m^3)	0.178	0.600
λ_l	Thermal conductivity (W/m K)	3.50×10^{-2}	0.680
η_l	Dynamic viscosity (kg/m s)	0.98×10^{-4}	2.88×10^{-4}
σ	Liquid–vapor surface tension (N/m)	0.12×10^{-3}	59×10^{-3}
γ	$\gamma = \partial\sigma/\partial T$ (N/m K)	0.093×10^{-3}	0.18×10^{-3}
T_c	Critical temperature (K)	5.25	647
H_l	Heat of evaporation (J/kg)	2.093×10^4	2.3×10^6
M	Molecular weight (kg/kmol)	4.002	18
a	Molecular core diameter (nm)	0.257	0.282
ε/k	Minimum potential of energy divided by Boltzmann constant (K)	10.8	231
T_{rew}	Olek et al. [12] rewetting temperature (°C) $T_{rew} \cong \sqrt{T_s \cdot T_c}$	−268.4	218.2

range of 100 nm). A grid of $n = 500$ points means that the size of each step is O(0.2 nm). Recall that the molecular size, a, defined in Eq. (A.7), is of the order of a few Angstroms. Clearly, this step size is close to the threshold of validity of the continuum picture. The convergence of the solution was tested by increasing the number, n, of grid points, until it became insensitive to further change in n. Similarly, the tolerance, E_T, was gradually decreased from 0.5 until the change in the solution profile became negligible.

The minimum acceptable number of grid points, for the case of water on stainless steel, was found to be greater than 13. Fig. 1(a) and (b) show the effect of increasing n from 20 to 40, and then from 60 to 100, on a plot of $h(\xi)$ versus ξ. Fig. 1(b) shows that for $n \geqslant 60$, the profile $h(\xi)$ is virtually independent of the number of grid steps. Thus, using a grid of 60 points ensures convergence of the profile solution in the water–stainless steel system. For other pairs of materials, satisfactory convergence was established at different values of $n \leqslant 100$. Therefore, $n = 100$ was selected for all materials studied in this work. Note that the wavy behavior of the interface profile (Fig. 1) will be discussed later.

The effect of the tolerance, E_T, was tested using the least accurate grid, $n = 20$ for the water–stainless steel system. The results in Fig. 1(c) show that no significant change in the solution is observable in the range $0.001 < E_T < 0.01$. Thus, it was decided that a grid of 100 points, with a tolerance value less than 0.01, produces an adequately convergent solution. A similar procedure was applied to determine n and E_T that produce convergent solutions for additional material combinations, such as different liquids on stainless steel. A plot of $h(\xi)$ versus ξ for helium on stainless steel is depicted in Fig. 2. This pair was selected as an example of a liquid having a very low saturation temperature at atmospheric pressure, as compared to the previously discussed example of water. For helium, $n = 60$ was determined as the minimum number of grid points that is required for satisfactory convergence. The reason for the difference in n for the two liquids results from the difference in their characteristic scales of the problem domain. The dimensionless numbers that characterize the interface equation may change significantly for different materials, and consequently, the numerical parameters also vary.

Note that this numerical testing procedure was carried out for all liquids under consideration, because the length scaling variable, L, depends on the characteristic molecular size, a, of each of them ($a^2 = A/6\pi\sigma$). Different fluids have different values of a and L ($L \equiv a/\theta_0^2$). For example, the scaling length for water is $L \cong 300$ nm, and that for helium is $L \cong 2100$ nm, which is seven times larger. Therefore, the minimum value of n needed for helium ($\cong 60$) is larger than that for water ($\cong 20$). This explains why larger number of grid points are required to ensure convergence in the case of helium as compared to that of water.

3.3. Effect of choice of boundary conditions

For the sake of brevity, the three boundary conditions of Eq. (22) are denoted by q_1, q_2 and q_3, as follows:

$$q_1 \equiv h_1(\xi = 0), \quad q_2 \equiv h_2(\xi = 0), \quad q_3 \equiv h_3(\xi = 0). \tag{24}$$

In order to check the effect of choosing different values of the three boundary conditions, two were held fixed, while the third one was allowed to vary. The first boundary condition tested was q_1, holding q_2 and q_3 fixed. It must have a minimum value which is greater than zero. Accordingly, the first estimate of the film thickness, q_1, was set at 0.2, this being equivalent to a few Angstroms. The parameter q_1 was increased by steps of 0.05 until the value of 0.65 was reached. In this

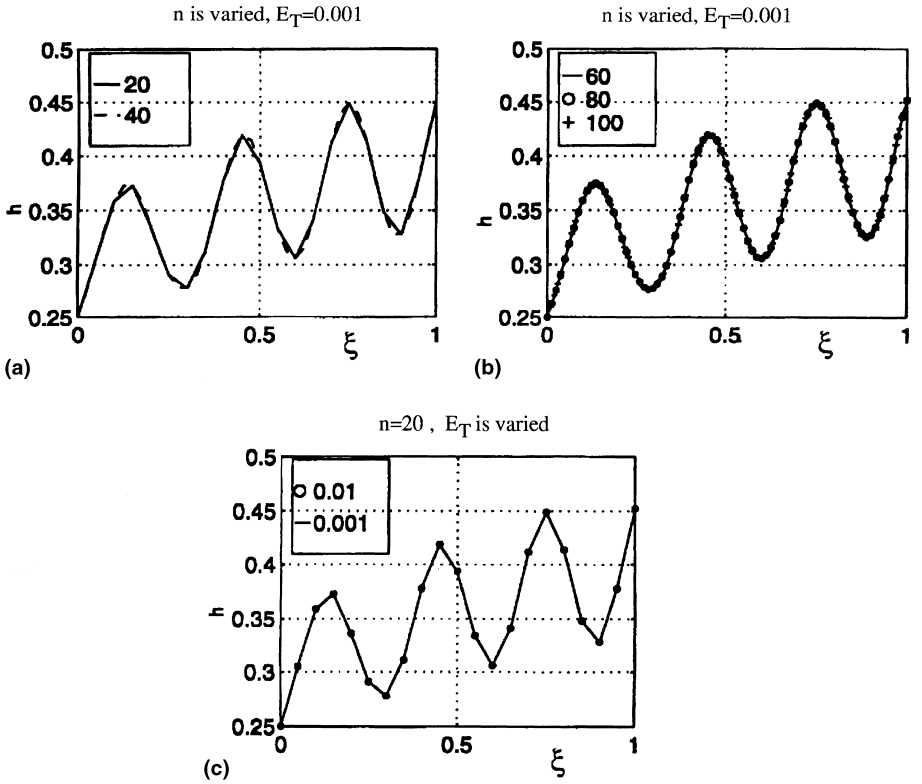

Fig. 1. Convergence test for the liquid–vapor interface profile, $h(\xi)$, for different number of grid points, n, (a) and (b), and for different values of the tolerance, E_T, (c). Water on stainless steel, parameters as in Eq. (23a) and boundary conditions as in Eq. (22).

range, an acceptable minimum value of q_1 was determined (see following analysis). The effects of q_2 and q_3 were examined similarly, using this value of q_1. The simulation combinations which were tested, are summarized in Table 2, and the respective profiles are shown in Figs. 3–5.

The three test cases specified in Table 2 cover a wide range of combinations of the boundary conditions. In case No. 1, the effect of q_1 on the solution behavior is studied, in order to determine its minimal value which still leads to a realistic solution. The results are shown in Fig. 3. The solution profiles, obtained for $0.2 \leqslant q_1 \leqslant 0.65$, show a wavy behavior. This is due to the evaporation of liquid packets at the interface. There is a substantial density change at the interface where the velocity of the evaporating liquid packets increases significantly in order to keep the mass balance. The force created due to the momentum change presses the liquid towards the solid, so that the interface becomes perturbed. This recoil effect is reported by Burelbach et al. [14], and its contribution to the momentum balance is expressed by the first term of Eq. (A.19). This term vanishes and no wavy profile develops for the case of uniform temperature field (see the solution for the isothermal case, Fig. 6). Note that in Fig. 3(a)–(d), as well as in most subsequent figures, the different ordinate scales provide enhanced resolution.

For $q_1 = 0.2$ (Fig. 3(a)), the shape of the film profile is significantly different from those obtained for larger values of q_1, in that the amplitude is much greater. This behavior is attributed to numerical stability of the solution.

All the solution profiles shown in Fig. 3(b)–(d) of O(1) are suitable for the scaling of the problem. The boundary condition $q_1 = 0.25$ was selected because it is the minimal value which provides a "stable" solution of the interface profile and in the range of interest. For smaller values of q_1, it is seen from Fig. 3 that the solution exhibits a strong wavy behavior, which can be attributed to numerical effects, magnifying the physical phenomena described above. The choice of $q_1 = 0.25$ eliminates this numerical influence.

Since the range of the dimensionless slope, q_2, is set between 0.1 and 1, it follows that $0.1° \leqslant \theta \leqslant 1°$. De Gennes et al. [11], in their analysis of the dynamic contact angle, found that its characteristic magnitude is of O(1°). Their analysis applies to a liquid at room temperature. Thus, for rewetting conditions a slope of 1° was taken as an upper limit of q_2. The interface solutions depicted in Fig. 4 seem to be independent of q_2. There-

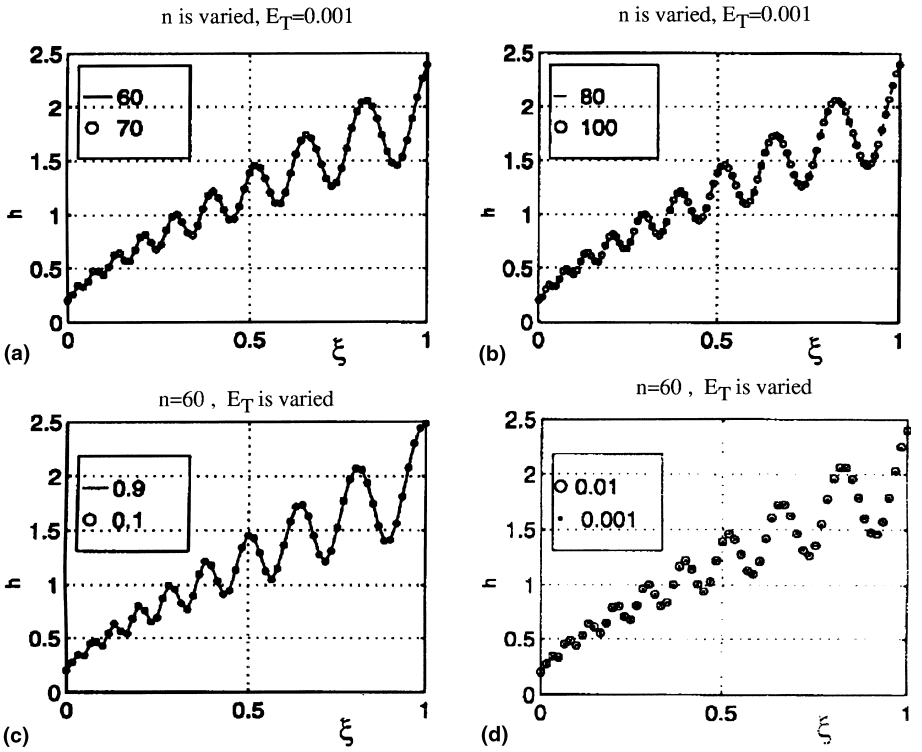

Fig. 2. Convergence test for the liquid–vapor interface profile, $h(\xi)$, for different number of grid points, n, (a) and (b), and for different values of the tolerance, E_T, (c) and (d). Helium on stainless steel, parameters as in Eq. (23b) and boundary conditions as in Eq. (22).

Table 2
Procedure for testing the boundary conditions parameters

Test case No.	Conditions of test			Step size	Upper limit of parameter tested	Parameter tested
	q_1	q_2	q_3			
1	0.2–0.65	1	1	0.05	0.65	q_1
2	0.2	0.1–1	1	0.1	1	q_2
3	0.2	1	1–10	1	10	q_3

fore, the upper limit of the range, at 1°, was selected as the boundary condition. Following the determination of q_1 and q_2, a wide range of values of q_3 was tested. Fig. 5 shows that the solution interface is practically independent of q_3. Therefore, the lowest value of $q_3 = 1$ was selected. The final set of the three boundary conditions is given in Eq. (22). Note that these boundary conditions were found to apply to the complete set of liquids that were tested in this work.

4. Results – quantitative analysis of the interface solution

The dimensionless parameters of the interface Eq. (16) were discussed qualitatively in Section 2. Eq. (16) comprises seven terms and contains seven dimensionless parameters ($\bar{A}$, N, C, F/C, u^*, S, F). The quantitative effects of each of the seven parameters were examined holding the remaining six parameters fixed. This did not apply to F/C (terms No. 2, 3 and 6 in Eq. (16)), which is not an independent variable, see Eq. (19). For the water–stainless steel system, subjected to the conditions discussed in Section 3, the reference values of the parameters are as in Eq. (23a). The thermo-physical properties of water are listed in Table 1.

As mentioned above, in the isothermal case Eq. (16) reduces to Eq. (18a). All the terms, which are involved with the temperature difference, ΔT, vanish. The relevant parameters that apply here are $\bar{A}$ and C, which express the solid–liquid intermolecular forces, and capillary and viscosity effects, and Eq. (18b) is identical to that derived by de Gennes [7]. Fig. 6(a) shows an example of the interface solution for this case, for water on stainless steel. The interface profile is smooth: the

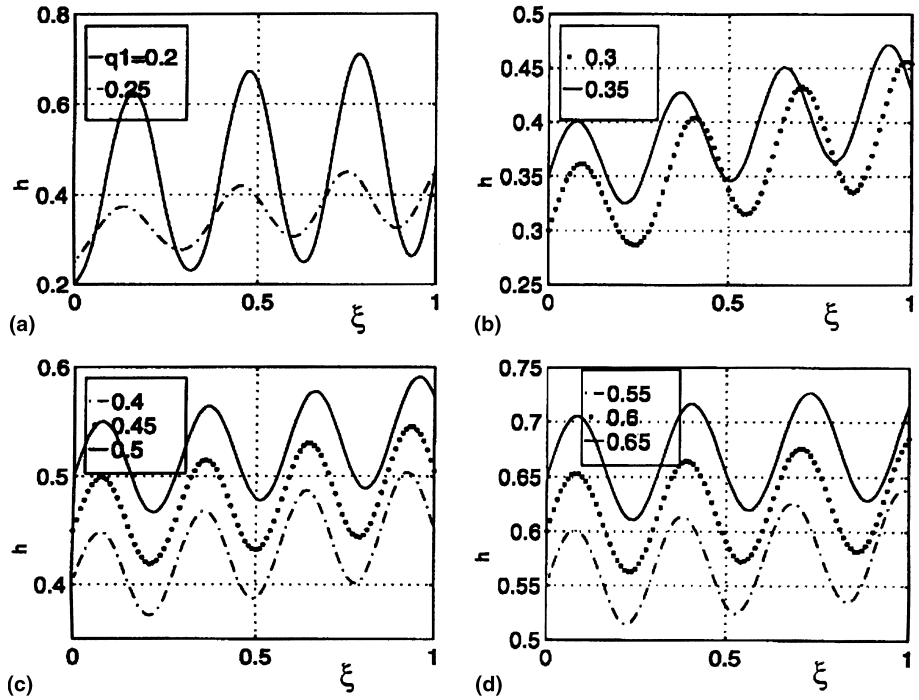

Fig. 3. The liquid–vapor interface profile, $h(\xi)$, for different values of the boundary condition q_1; $q_2 = q_3 = 1$, see Table 2: (a) $q_1 = 0.2$, 0.25; (b) $q_1 = 0.3$, 0.35; (c) $q_1 = 0.4$, 0.45, 0.5; (d) $q_1 = 0.55$, 0.6, 0.65.

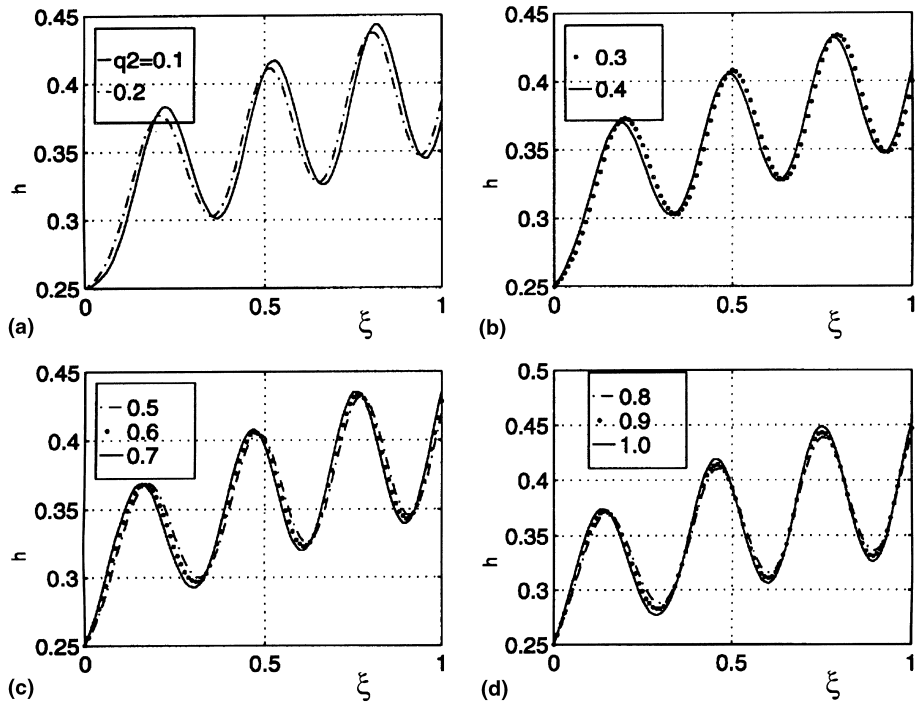

Fig. 4. The liquid–vapor interface profile, $h(\xi)$, for different values of the boundary condition q_2; $q_1 = 0.25$, $q_3 = 1$, see Table 2: (a) $q_2 = 0.1$, 0.2; (b) $q_2 = 0.3$, 0.4; (c) $q_2 = 0.5$, 0.6, 0.7; (d) $q_2 = 0.8$, 0.9, 1.0.

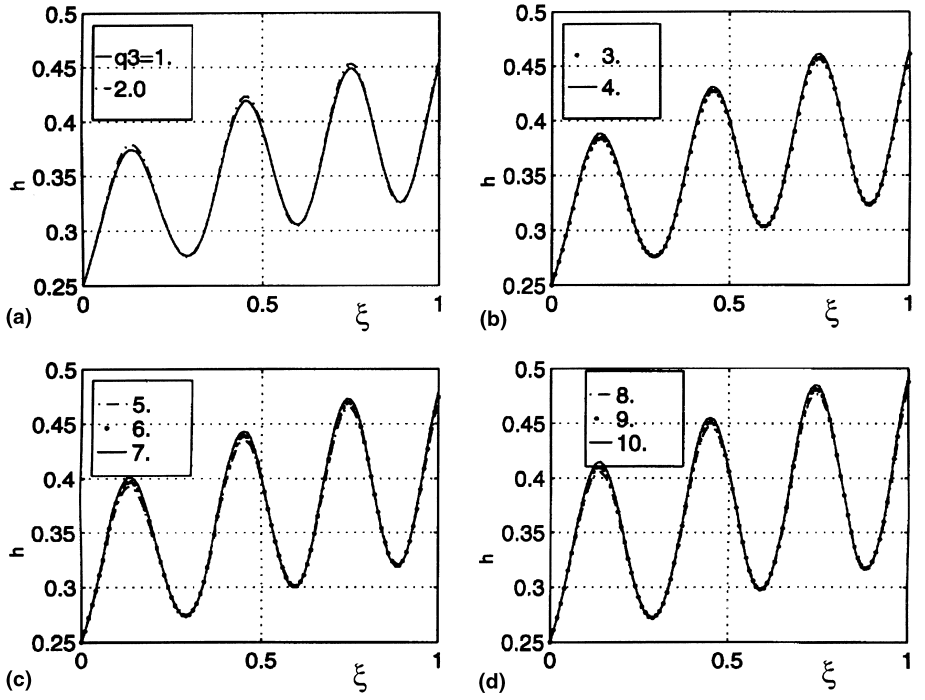

Fig. 5. The liquid–vapor interface profile, $h(\xi)$, for different values of the boundary condition q_3; $q_1 = 0.25$, $q_2 = 1$, see Table 2: (a) $q_3 = 1$, 2.0; (b) $q_3 = 3$, 4; (c) $q_3 = 5$, 6, 7; (d) $q_3 = 8$, 9, 10.

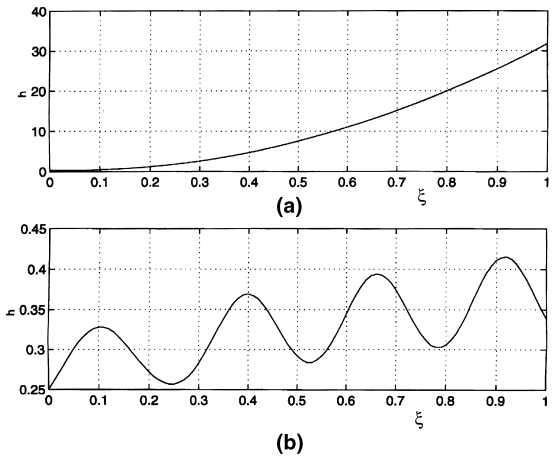

Fig. 6. Solution of the interface profile, $h(\xi)$; water on stainless steel (reference parameters, Eq. (23a)): (a) Isothermal conditions, $\Delta T = 0$, de Gennes Eqs. (18a) and (18b). (b) Non-isothermal conditions of rewetting, $\Delta T = 160°C$, present model, Eq. (16).

elimination of the surface undulation is a consequence of absence of the recoil effect, as discussed above. The film thickness in the non-isothermal case ($\Delta T \neq 0$, Fig. 6(b)), is wavy and much smaller than that for the isothermal one ($\Delta T = 0$, Fig. 6(a)). This is mainly due to intensive evaporation. Furthermore, the decrease of the surface tension leads to a flatter film (moderate slope of the interface), and spreading of the film on the hot surface is enhanced. The liquid is attracted to the solid more strongly by the intermolecular forces, as expressed by the term $3C\bar{A}h_\xi/h^4$ in Eq. (16). The contribution of the denominator at small values of h becomes dominant.

A parametric study was performed concerning the effects of the dimensionless parameters in Eq. (16) on the solution of the interface, $h(\xi)$. The reference values of these parameters for water on stainless steel are specified in Eq. (23a). The effect of the velocity was considered using the variation of the capillary number C. Each parameter was tested holding the other parameters fixed. The results of the parametric tests are depicted in Figs. 7–11.

4.1. Capillary number, C

A large value of the capillary number, C, indicates that the viscous forces are stronger than the capillary forces which arise due to the interfacial surface tension, σ. Increase of either the viscosity, η, or the velocity, U_0, results in an increase of the capillary number. Fig. 7(a)–(d) show interface profile solutions, $h(\xi)$, obtained for several values of C, in the range 0.38–1.49. Smaller

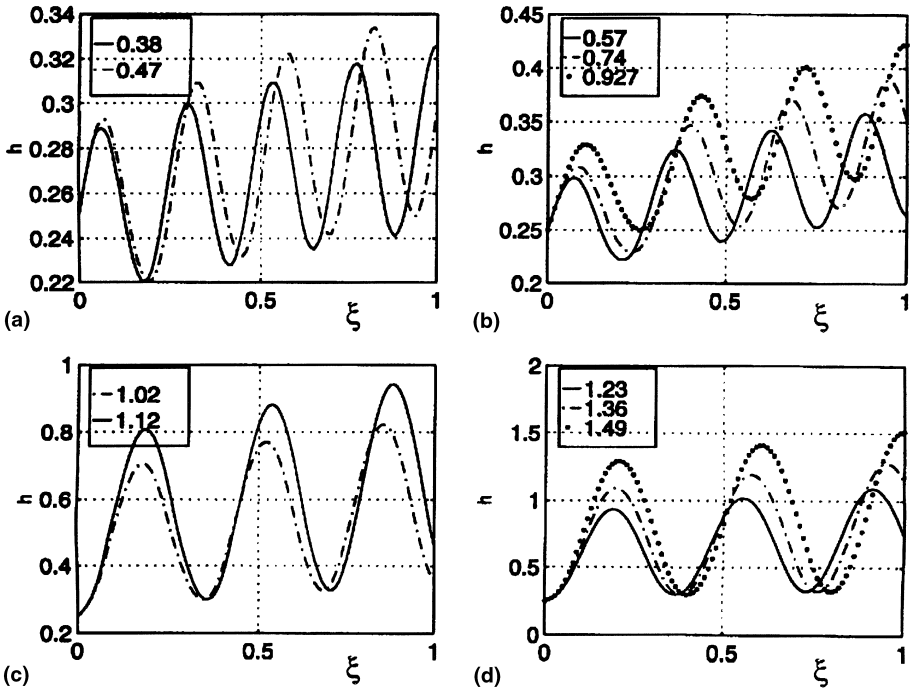

Fig. 7. Effect of the capillary number, C, on the solution profile, $h(\xi)$, of Eq. (16): (a) $C=0.38$, 0.47; (b) $C=0.57$, 0.74, 0.927; (c) $C=1.02$, 1.12; (d) $C=1.23$, 1.36, 1.49. Reference value: $C=0.927$.

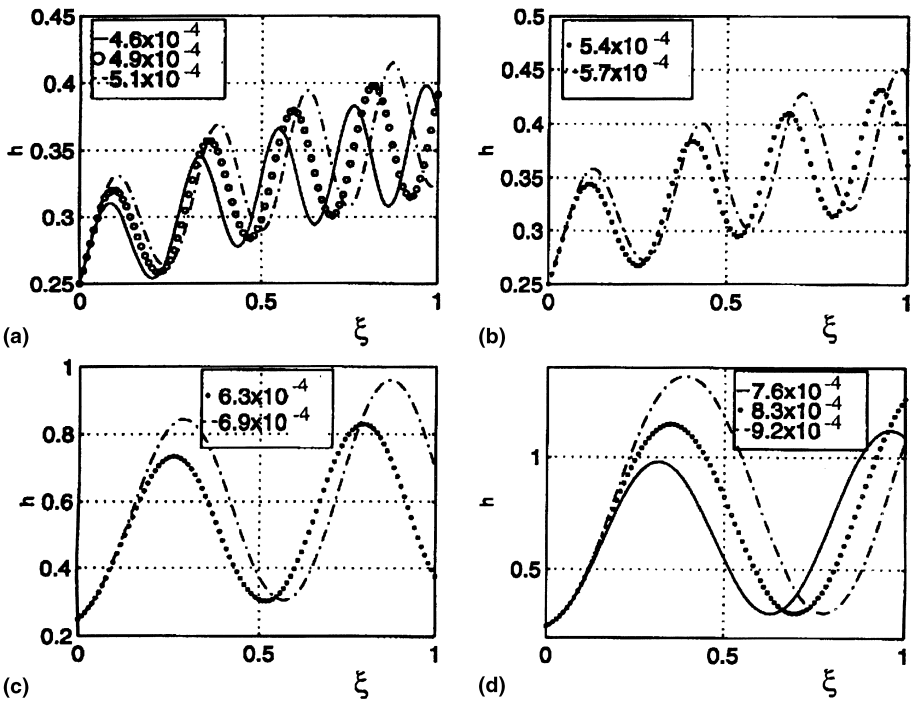

Fig. 8. Effect of the thermo-capillary number, $C\theta_0^2/F$, on the solution profile, $h(\xi)$, of Eq. (16): (a) $TC=4.6$, 4.9, 5.1; (b) $TC=5.4$, 5.7; (c) $TC=6.3$, 6.9; (d) $TC=7.6$, 8.3, 9.2. Reference value: $C\theta_0^2/F = 5.7\times10^{-4}$. $TC = (C\theta_0^2/F)\times10^4$.

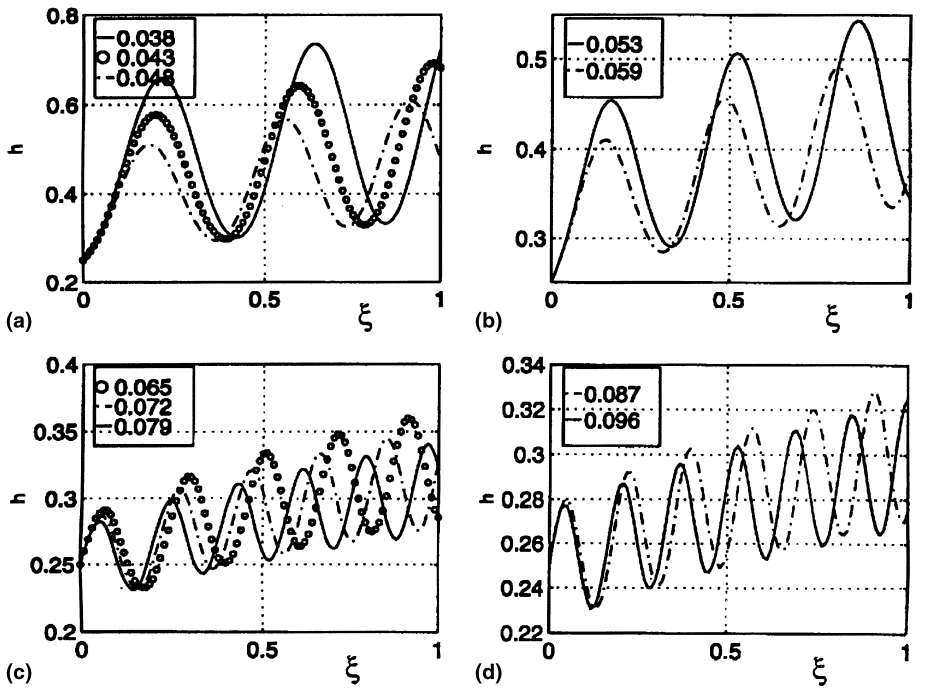

Fig. 9. Effect of the factor N on the solution profile, $h(\xi)$, of Eq. (16): (a) $N = 0.038$, 0.043, 0.048; (b) $N = 0.053$, 0.059; (c) $N = 0.065$, 0.072, 0.079; (d) $N = 0.087$, 0.096. Reference value: $N = 6.5 \times 10^{-2}$.

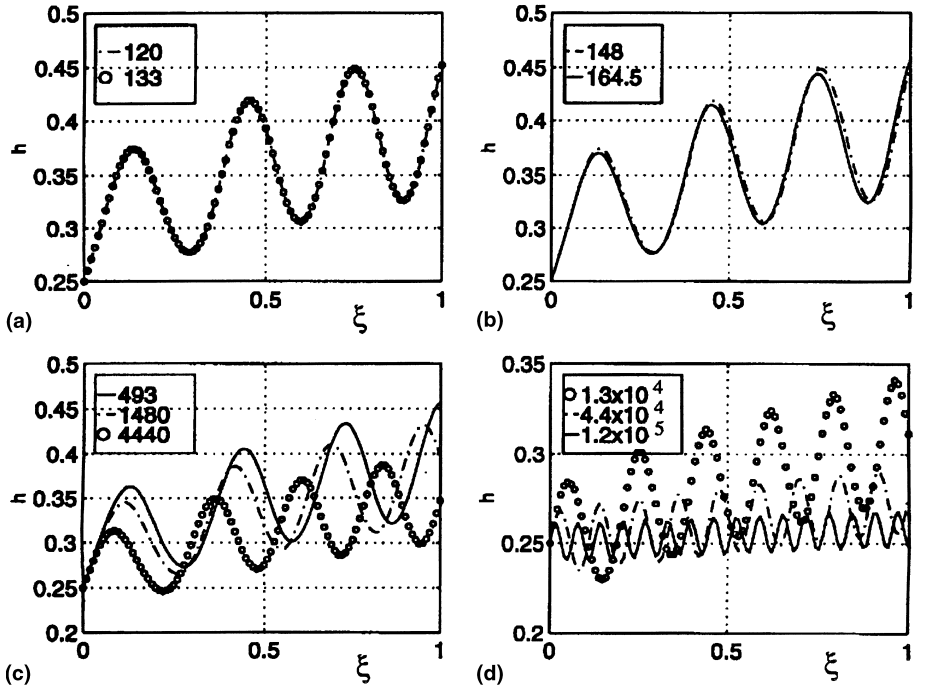

Fig. 10. Effect of the evaporation coefficient, S, on the solution profile, $h(\xi)$, of Eq. (16): (a) $S = 120$, 133; (b) $S = 148$, 164.5; (c) $S = 493$, 1480, 4440; (d) $S = 1.3 \times 10^4, 4.4 \times 10^4, 1.2 \times 10^5$. Reference value: $S = 164.5$.

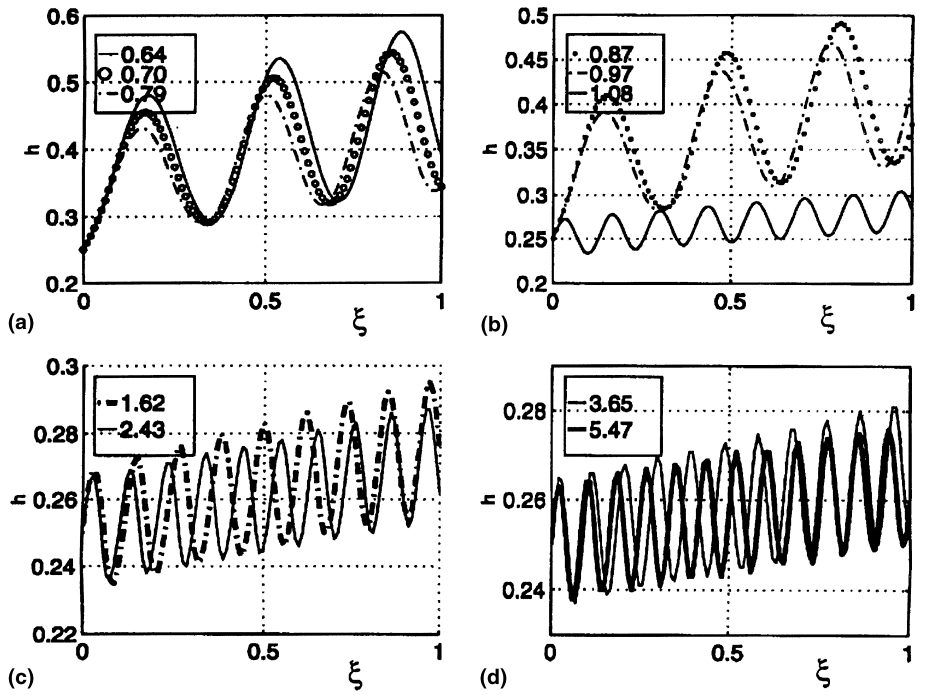

Fig. 11. Effect of the solid–liquid intermolecular force term, $\bar{A}$ on the solution profile, $h(\xi)$, of Eq. (16). (a) $\bar{A} = 0.64, 0.70, 0.79$; (b) $\bar{A} = 0.87, 0.97, 1.08$; (c) $\bar{A} = 1.62, 2.43$; (d) $\bar{A} = 3.65, 5.47$. Reference value: $\bar{A} = 1.08$.

values of C produce flatter interface profiles, e.g., the profile peaks become smaller. For example, at $C = 1.49$, the highest peak of h is close to 1.5 (Fig. 7(d)), while at $C = 0.38$ (Fig. 7(a)) it is close to 0.33. A simple explanation for this behavior (in terms of effect of the velocity) is that for smaller values of U_0, the flow rate is lower. Another explanation for this phenomenon (of flatter profile for lower C) is based on the force balance on the liquid. Suppose C is decreased as a result of decrease in the viscosity, η. If this would have been the only change, with the rest of the dimensionless parameters fixed, all the forces would remain the same, the viscous force inclusively. Then for lower values of η, the velocity distribution must involve larger gradients at the wall, and hence, at the same value of U_0, the film thickness must be smaller (flatter profile). Note, however, that a decrease in η means that the thermo-capillary parameter, F/C, and the Hamaker constant $\bar{A}$ are also affected. In order to hold the former constant, as is done here, η is postulated to decrease. This leads to a higher value of the surface tension, σ. In order to hold $\bar{A}$ constant, a decrease in the parameter A (dimensional) is also postulated.

The term $\bar{A}/h^3$ contributes to the liquid pressure. The pressure forces near the contact line, which result from the solid–liquid intermolecular attraction, counteract the shear and capillary forces. If $\bar{A}$ is held fixed, then the pressure in the film increases in proportion to $1/h^3$. The pressure is related to the slope, h_ξ, which results from the pressure gradient, $\partial(\bar{A}/h^3)/\partial\xi$. In order to hold the pressure fixed, the slope, h_ξ, should be decreased and consequently the film becomes flatter. Note that the force, resulting from the change in $\sigma(\Theta)$, is small relative to the viscous and solid–liquid attraction forces.

4.2. Thermo-capillary number, $C\theta_0^2/F$

The effect of the thermo-capillary number, $C\theta_0^2/F$, on the solution profile is examined by changing its value in the range 4.6×10^{-4}–9.2×10^{-4} (Fig. 8). As can been seen, larger values of $C\theta_0^2/F$ entail steeper profiles. A high value of $C\theta_0^2/F$ indicates dominance of the viscous forces over the thermo-capillary forces which are caused by temperature gradients. Increasing the viscosity, η, or the velocity, U_0, increases the thermo-capillary number. If the temperature difference, ΔT, is increased, the value of $C\theta_0^2/F$ becomes smaller and the thermo-capillary forces turn more dominant. If the solid temperature, T_w, is increased, the liquid temperature also increases, and the liquid–vapor interfacial tension, $\sigma(\Theta)$, decreases. Consequently, the forces that pull the film backwards are diminished, and hence the film is thicker as expected, see Fig. 8(d).

Furthermore, an increase of $C\theta_0^2/F$ by a factor of 2 (from 4.6×10^{-4} to 9.2×10^{-4}) yields a threefold rise in the maximum peak value of the profile (Fig. 8(d)).

4.3. The factor N

The dimensionless factor N, which appears in the constitutive relations is one of the parameters involved with the evaporation process. This factor includes liquid properties such as molecular weight, thermal conductivity, heat of evaporation and temperature. Larger values of N mean that the evaporation at the interface becomes more intensive. This agrees with the fact that smaller values of the saturation temperature, T_s, lead to higher values of N. Fig. 9 shows the effect of N, in the range 0.038–0.096.

Larger values of N lead to flatter films and their undulating or "wavy" behavior is intensified, see Fig. 9(d), where the undulation frequency is highest. An increase of N means also an increase of the mass flux, j, across the interface, Eq. (A.18). This flux appears in the force balance at the interface in the normal direction, see Eq. (A.19). At large values of j, the force expressed by the left term of this equation, $-Sj^2$, becomes more dominant, and consequently the liquid–vapor interface is "drawn" towards the solid. In this case, a flatter film is expected, as can be seen, indeed, in Fig. 9. The forces resulting from the liquid pressure, p, counteract the force caused by, j^2, and due to the incompressibility of the liquid and surface tension, the interface is "forced" to be curved.

The third component in this force balance is the capillary force, which increases with the curvature, $h_{\xi\xi}$. It is clear that along the undulating interface, the sign of the curvature changes. In this context, the capillary forces act to balance the two forces mentioned above. For example, at the maxima points, where the film thickness is larger, the expected mass flux $j = N\Theta^{\mathrm{I}}$ is smaller because the interface temperature, Θ^{I}, is lower. At these points, the forces due to the liquid pressure, p, exceed those due to j^2. Therefore the capillary forces must be directed toward the solid, resulting in a positive curvature. At the minima points, the reverse picture applies (the liquid pressure is smaller), and hence, the direction of the capillary forces is towards the vapor phase, so that the curvature is negative.

4.4. The evaporation coefficient, S

The fourth term of Eq. (16) includes the dimensionless parameter S, which originates from the normal stress balance, Eq. (A.19). Larger values of S appear in situations that involve higher temperature gradients. S expresses the ratio between the conducted heat flux, $(\lambda_l \Delta T)/(L\theta_0)$, and that related to the evaporation $(L/(H_l^2 \sigma \rho_v \theta_0))$. The S values were changed in the range 120–1.2×10^5, and the corresponding solution profiles are shown in Fig. 10. Larger values of S (Fig. 10(d)) lead to flatter films with higher undulation frequency. This behavior can be explained using arguments similar to those applied above to the effect of N. This conforms with S being a part of the recoil effect term. Moreover, since both N and S appear in the fourth term of Eq. (16), the effect of this term on the tendency of the solution profile to be flatter is expected to be more significant.

4.5. Solid–liquid intermolecular forces, $\bar{A}/h^3$

The solid–liquid molecular interaction is expressed by the term $\bar{A}h_\xi/h^4$ in Eq. (16). The Hamaker constant, A, usually ranges between 0.7×10^{-21} and 5×10^{-19} J. In this work, its value was taken as 10^{-20} J, following the postulate of Burelbach et al. [14]. Higher values of $\bar{A}$ mean stronger interaction, or attraction, between the solid and liquid molecules. Fig. 11 shows solution profiles that were plotted for $\bar{A}$ in the range 0.64–5.47. Increase of $\bar{A}$ flattens the profile and concurrently its undulation frequency increases. Thus, $\bar{A}$ also contributes to the surface perturbation in conjunction with N and S.

5. Summary and conclusions

This paper describes the development of a novel approach and a new method to characterize rewetting phenomena. The basic foundation of the approach appears in [1], which defines the physical (hydrodynamic) micro-scale model, and includes the derivation of the governing equations and boundary conditions of the mathematical model. In the present paper, this model is used to develop the interface equation for the thickness, h, of the liquid film, as a function of the distance from its leading edge. The full comprehensive equation appears in Appendix B, while in the text a simplified form is derived, in a coordinate frame moving with the contact line, $\xi = x - u^* t$. It is emphasized that these interface equations were developed for a non-isothermal situation, including effects of evaporation, thermo-capillary and inter-molecular forces between the liquid and solid. The new approach is a generalization of de Gennes [7] for the case of uniform temperature, and our interface equation reduces, indeed to his, for the particular case of isothermal conditions. The third-order differential equation for $h(\xi)$ was solved numerically. The effects of the numerical parameters on convergence and behavior of the solution were investigated. This was done for many solid–liquid pairs and demonstrated here for two pairs, with large disparity between their properties: water on stainless steel and helium on stainless steel. It was found that the solution profiles converged at relatively small number of grid points. This is a good indication that solutions for other systems, with intermediate thermophysical properties, will be convergent as well. A grid consisting of $n \geqslant 60$ points, and setting the relative accuracy (tolerance) at $E_T \leqslant 0.01$, provided convergence for all systems investigated. The effects of selecting the

boundary conditions were also considered. The set $h(\xi) = 0.25,\ h_\xi = 1$, and $h_{\xi\xi} = 1$ at $\xi = 0$, guarantees a convergent and stable solution profile of the interface.

A parametric study was carried out in order to evaluate the effects of the various dimensionless parameters that appear in the interface equation. Their values were taken for a water/stainless steel system presented here as a reference case. Decrease of the capillary number, C, drives the solution of the interface toward flatter profiles. This behavior can be explained by realizing that for lower values of the quench velocity, U_0, the flow rate is smaller. Another explanation for this phenomenon is based on the force balance on the liquid. A decrease of C can be caused by a decrease in the viscosity, η. If this is the only change, e.g., with all other dimensionless parameters held fixed, then all the forces that act on the liquid would have remained the same, inclusive of the viscous force. For a lower value of η, the velocity distribution must have a larger gradient at the wall, and hence, at fixed U_0, the film thickness must be smaller (flatter profile).

Larger values of $C\theta_0^2/F$, which stands for thermo-capillary effects, lead to steeper solution profiles of the interface. If the temperature difference, ΔT, is increased, the value of C/F decreases, and the thermo-capillary forces become more dominant. Recall that these forces act so as to pull the film backwards, and as they are diminished, the film is expected to be thicker. Furthermore, an increase of $C\theta_0^2/F$ by a factor of 2, results in a three-fold increase in the highest peak of the solution profile of the interface. This means that the solution profile is sensitive to changes in $C\theta_0^2/F$.

The factor N, which reflects the effect of liquid properties, such as molecular weight and thermal conductivity, influences the solution profile considerably. Larger values of N indicate higher evaporation rates and mass fluxes across the interface. In this case, the solution profile of the interface becomes flatter. This reflects the recoil effect due to the mass flux that presses the film down towards the solid. Consequently, for larger values of N, a flatter film is obtained and its undulating or wavy behavior is intensified. At higher temperature gradients, both the interface temperature, Θ^1, and the undulation frequency increase. In this context, the higher mass fluxes, that push the liquid towards the solid, are responsible for enhanced wavy behavior of the interface. The evaporation coefficient S, which originates from the normal stress balance, affects the solution profile in a similar way. Larger values of S lead to flatter films, and at the same time their effect on the frequency of undulation of the interface becomes stronger. The effect of the solid–liquid intermolecular force term, $\bar{A}h_\xi/h^4$, was tested by changing the dimensionless Hamaker constant, $\bar{A}$. Larger values of $\bar{A}$ produce a flatter profile, and surface undulation of higher frequencies.

The new equation of the solid–liquid interface and its parametric analysis, facilitate further insight concerning hydrodynamic mechanisms that are involved in motion of thin liquid films on hot solid surfaces, under conditions of high temperature gradients and intense evaporation. This gives the hydrodynamic foundation for analysis of rewetting phenomena and the definition of the quench temperature and velocity, that are discussed in the subsequent part of this series.

Appendix A. The non-isothermal microscale hydrodynamic model

The first stage in the development of the general theoretical method for the simultaneous determination of rewetting velocity and temperature involved the derivation of a non-isothermal microscale hydrodynamic model, Ben David et al. [1]. The basic approach which is outlined in this Appendix, includes a brief summary of the underlying assumptions, the scaling of model parameters, balance equations and boundary conditions.

We present here the balance equations governing the velocity and temperature field, in the liquid layer which flows behind the moving quench front. The layer configuration is illustrated in Fig. 12. Following de Gennes et al. [11] the rewetting process is dominated by the "proximal" region in this layer, where intermolecular forces (mainly van der Waals) and capillary effects are significant.

The basic assumptions of the hydrodynamic microscale model are as follows:

1. The analysis is focused on the domain close to the contact line, which is of the order of 100 Å (10 nm), and 1000 Å (100 nm), in the vertical direction (film thickness), and the horizontal direction (parallel to the solid surface), respectively.
2. The thin viscous liquid film is bounded by its vapor (gas phase), and by a rigid wall at constant temperature.
3. The liquid film is thin enough so that gravitational effects are negligible, and van der Waals attraction forces are significant. However, the film thickness still warrants description of the liquid as a continuum and use of related flow theories.
4. The liquid film consists of an incompressible Newtonian fluid.
5. The liquid properties, i.e., density, viscosity, etc., except for the surface tension, do not change significantly with temperature, and their values are taken as those under conditions of saturation temperature at atmospheric pressure.
6. The liquid in the film evaporates. Consequently, there is heat, mass, and momentum transfer at the liquid–vapor interface. The evaporation dynamics is described by boundary condition jumps.

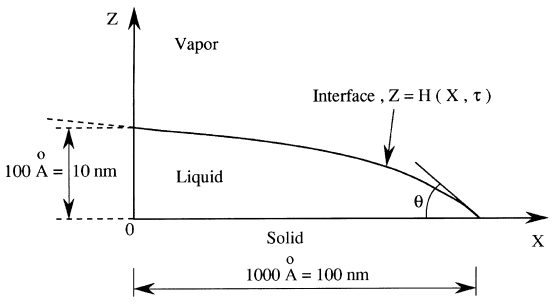

Fig. 12. Sketch of problem geometry.

7. The density, viscosity, and thermal conductivity are assumed to be considerably greater in the liquid as compared to the vapor, so that the dynamics of the vapor can be decoupled from that of the liquid. This justifies the adoption of the one-sided model simplification.
8. Surface phenomena such as contact angle, capillary and thermocapillary effects are significant.
9. The rewetting geometry is two-dimensional due to the fact that the liquid film thickness is considerably smaller than its longitudinal dimension.
10. The small slopes ($\theta \ll 1$), which are characteristic of the liquid–vapor interface in rewetting situations, allow the use of the lubrication approximation.
11. The three-phase contact line moves at a nearly constant velocity, U_{rew}, so that in the moving frame of this contact line, the problem can be described as being quasi-static.
12. When the temperature at the three-phase contact line exceeds the rewetting temperature, which is independent of time and space, no solid–liquid contact is possible.

The balance equations (continuity, momentum and energy), and boundary conditions, for the liquid layer domain under consideration, are presented in dimensionless form. The corresponding scaling procedure, and simplifications resulting from the above assumptions, are outlined below.

The pressure derivatives in the momentum equations are those of the generalized pressure, defined by

$$P = P_{\mathrm{hyd}} + \Phi, \tag{A.1}$$

where P_{hyd} is the hydrodynamic pressure, and Φ denotes a potential associated with the Van der Waals attraction forces

$$\Phi = \Phi(H) = -A/H^3 + A/Z^3. \tag{A.2}$$

The boundary conditions at the wall, $Z = 0$, are zero velocity ($U = W = 0$) and constant temperature $T = T_{\mathrm{w}}$. At the interface, $Z = H(X, \tau)$, liquid–vapor jump conditions are applied. The mass flux, J, which appears in these conditions, is defined by

$$J = \rho_{\mathrm{l}}(\mathbf{V}_{\mathrm{l}} - \mathbf{V}^{\mathrm{I}}) \cdot \mathbf{n} = \rho_{\mathrm{v}}(\mathbf{V}_{\mathrm{v}} - \mathbf{V}^{\mathrm{I}}) \cdot \mathbf{n}, \tag{A.3}$$

where $\boldsymbol{n}$ is the normal unit vector, and $\boldsymbol{V}^{\mathrm{I}}$ is the velocity of the interface, whose modulus is equal to $\mathrm{d}H/\mathrm{d}\tau$. This leads to the linearized relation

$$J = \rho_{\mathrm{l}}(-H_\tau - UH_X + W). \tag{A.4}$$

The mass flux can also be expressed by the linearized, kinetic, constitutive relation

$$J = \left(\frac{\alpha\rho_{\mathrm{v}}H_{\mathrm{l}}}{T_{\mathrm{s}}^{3/2}}\right)\left(\frac{M}{2\pi R_{\mathrm{g}}}\right)^{1/2}\left(T^{\mathrm{I}} - T_{\mathrm{s}}\right). \tag{A.5}$$

The normal stress boundary condition at the interface is written as a jump momentum balance, including the surface tension $\sigma(T)$. The shear stress boundary condition includes, then, the gradient of $\sigma(T)$ along the interface, owing to its dependence on the temperature, i.e., thermo-capillary effect. The energy balance, representing the boundary condition at the interface, includes the heat of evaporation, kinetic energy exchange, heat conduction in the two phases, and rate of work due to viscous stresses and deformation.

The governing equations and boundary conditions are transformed into dimensionless forms by the following scaling procedure. The dimensionless lengths, x and z, and film thickness, h, are defined by:

$$x = \frac{X}{L}, \qquad z = \frac{Z}{L\theta_0}, \qquad h = H/L\theta_0, \tag{A.6}$$

$$L = a/\theta_0^2, \quad a = (A/6\pi\sigma)^{1/2}, \tag{A.7}$$

where a is a convenient representative molecular size, and θ_0 is a reference contact angle, which is typically very small, O(1°).

The horizontal velocity is scaled by a reference spreading velocity $U_0 = K\theta_0^m$, where $m = 3$ and K is of the order of 10^3 m/s. Thus, $U_0 \equiv 0.01$ m/s is selected. The horizontal and vertical velocity components are then scaled in accordance with the continuity equation

$$u = U/U_0, \quad w = W/U_0\theta_0. \tag{A.8}$$

The time scale follows from the choice of the length and velocity scales

$$t = \tau U_0/L. \tag{A.9}$$

The pressure scale is obtained by expressing a balance between pressure and viscous forces. This yields

$$p = \left(\frac{L\theta_0^2}{\eta_{\mathrm{l}}U_0}\right)P, \quad \phi = \left(\frac{L\theta_0^2}{\eta_{\mathrm{l}}U_0}\right)\Phi, \tag{A.10}$$

where

$$p = p_{\mathrm{hyd}} + \phi = p_{\mathrm{hyd}} - \bar{A}/h^3 + \bar{A}/z^3 \tag{A.11}$$

and $\bar{A}$ is the dimensionless Hamaker constant. The temperature field is scaled through

$$\Theta = \frac{T - T_s}{T_w - T_s}, \tag{A.12}$$

where T_w and T_s are the wall and saturation temperatures.

The balance equations of mass, momentum and energy, obtained by applying the above model assumptions, simplifications and scaling, are as follows:

$$\frac{\partial u}{\partial x} + \frac{\partial w}{\partial z} = 0, \tag{A.13}$$

$$-\frac{\partial p}{\partial x} + \frac{\partial^2 u}{\partial z^2} = 0, \tag{A.14}$$

$$\frac{\partial p}{\partial z} = 0, \tag{A.15}$$

$$\frac{\partial^2 \Theta}{\partial z^2} = 0. \tag{A.16}$$

The boundary conditions at the wall are

$$u = 0, \quad w = 0, \quad \Theta = 1 \quad \text{at } z = 0. \tag{A.17}$$

The dimensionless mass flux at the interface, is obtained from a balance of heat of vaporization and heat conducted in the liquid

$$j = N\Theta^{I}, \tag{A.18}$$

where Θ^{I} is the interface temperature. Note that N and the following dimensionless groups are defined in the nomenclature.

The dimensionless boundary conditions at the interface, of normal and shear stresses and of energy are:

$$-Sj^2 + Cp = -\frac{\partial^2 h}{\partial x^2}\left(1 - F\Theta^{I}\right) \quad \text{at } z = h, \tag{A.19}$$

$$\frac{C\theta_0^2}{F}\frac{\partial u}{\partial z} = -\left(\frac{\partial \Theta}{\partial x} + \frac{\partial \Theta}{\partial z}\frac{\partial h}{\partial x}\right) \quad \text{at } z = h, \tag{A.20}$$

$$N\Theta^{I} + \frac{\partial \Theta}{\partial z} = 0 \quad \text{at } z = h. \tag{A.21}$$

Finally, the kinematic condition of mass balance at the interface yields

$$EN\Theta^{I} = w - \frac{\partial h}{\partial t} - u\frac{\partial h}{\partial x} \quad \text{at } z = h. \tag{A.22}$$

Appendix B. Derivation of an interface equation and analytical solutions of the temperature and flow fields

The model equations, as given in Appendix A, can be solved analytically. The temperature and flow fields can be solved in terms of the interface profile, $h = h(x,t)$, which as yet is unknown.

B.1. Temperature field

The solution for the dimensionless temperature field is given by Eq. (2), as a linear profile,

$$\Theta(x,z,t) = c_1 z + c_2. \tag{B.1}$$

Using the boundary conditions; see Eqs. (A.17) and (A.21)

$$z = 0: \quad \Theta = 1, \tag{B.2}$$

$$z = h: \quad \Theta_z + N\Theta = 0, \tag{B.3}$$

c_1 is obtained as a function of $h(x,t)$,

$$c_1(x,t) = -\frac{N}{Nh + 1} \tag{B.4}$$

and

$$c_2 = 1. \tag{B.5}$$

Substituting Eqs. (B.4) and (B.5) into Eq. (B.1), gives

$$\Theta(x,z,t) = \frac{1 + N(h(x,t) - z)}{1 + Nh(x,t)}. \tag{B.6}$$

Hence, the temperature, Θ, at the liquid–vapor interface, $z = h(x,t)$, is given by

$$\Theta^{I} = \frac{1}{1 + Nh}. \tag{B.7}$$

B.2. Formulation of the interface equation

By virtue of continuity, see Eq. (A.13), and integration across the liquid layer, the following expression is obtained:

$$-\int_0^h u_x \, dz = w|_0^h = w(h) - w(0), \tag{B.8}$$

where $w(h)$ and $w(0)$ is the vertical component of the velocity at $z = h$ and $z = 0$, respectively.

Substitution of the no-penetration (rigid-wall) boundary condition, Eq. (A.17), and using the Leibnitz rule, expression (B.8) may be presented as

$$u_{z=h}h_x - \frac{\partial}{\partial x}\int_0^h u \, dz = w_{z=h}. \tag{B.9}$$

The vertical velocity component, w, at $z = h$, is given by the kinematic boundary condition, see Eqs. (A.4), (A.5) and (A.22). Therefore, substitution of Eq. (B.9) into Eq. (A.22) leads to

$$h_t + EN\Theta^{I} + \frac{\partial}{\partial x}\int_0^h u \, dz = 0. \tag{B.10}$$

The velocity, u, is obtained by solving the momentum balance in the x direction, Eq. (A.14)

$$u_{zz} = p_x, \tag{B.11}$$

where the generalized pressure p includes the solid–liquid potential of interaction, ϕ, see Eqs. (A.1), (A.2) and (A.11). The pressure distribution is given by Eq. (15)

$$p(x,z,t) - p_g = -\frac{1}{C}\left[h_{xx}(1 - F\Theta^I) - Sf^2\right] - \frac{\bar{A}}{h^3} + \frac{\bar{A}}{z^3}, \tag{B.12}$$

where p_g is arbitrarily set to zero.

Using Eq. (A.18) for the mass flux and Eq. (B.7) for the interface temperature, Θ^I, and substituting the pressure from Eq. (B.12) into the momentum balance (B.11), gives

$$u_{zz} = \frac{1}{C}\left[-h_{xxx}\left(1 - \frac{F}{1+Nh}\right) - \frac{FNh_{xx}h_x}{(1+Nh)^2} - \frac{2SN^3h_x}{(1+Nh)^3}\right] + \frac{3\bar{A}h_x}{h^4}. \tag{B.13}$$

The velocity component, u, is obtained by double integration of Eq. (B.13).

$$u(x,z,t) = f_1(x,t)z^2 + f_2(x,t)z + f_3(x,t), \tag{B.14a}$$

where

$$f_1(x,t) = \frac{1}{2C}\left[-h_{xxx}\left(1 - \frac{F}{1+Nh}\right) - \frac{FNh_{xx}h_x}{(1+Nh)^2} - \frac{2SN^3h_x}{(1+Nh)^3}\right] + \frac{3\bar{A}h_x}{2h^4} \tag{B.14b}$$

and $f_2(x,t)$ and $f_3(x,t)$, which do not depend on the variable z, are determined through the boundary conditions for the velocity, at $z = 0$ and $z = h$.

At the solid, $z = 0$, application of the no-slip condition, as given by Eq. (A.17), gives

$$u(x, z = 0, t) = f_3(x,t) = 0. \tag{B.15}$$

The tangential-stress boundary condition at $z = h$, see Eq. (A.20), is used to determine $f_2(x,z)$

$$\frac{C\theta_0^2}{F}u_z\big|_{z=h} = -(\Theta_x + \Theta_z h_x)\big|_{z=h}, \tag{B.16a}$$

where $C\theta_0^2/F$ is the thermo-capillary number [1].

At $z = h$, substitution of the derivatives of the temperature function, see Eq. (B.6), with respect to z and x, into Eq. (B.16a), gives,

$$u_z = \frac{FNh_x}{C\theta_0^2(1+Nh)^2}, \quad z = h \tag{B.16b}$$

According to the velocity function, Eq. (B.14a), the following expression for u_z, at $z = h$, is derived:

$$u_z = 2f_1(x,t)z + f_2(x,t)\big|_{z=h} = 2f_1(x,t)h + f_2(x,t). \tag{B.17}$$

Solving Eqs. (B.16b) and (B.17) for $f_2(x,t)$ yields

$$f_2(x,t) = \frac{FNh_x}{C\theta_0^2(1+Nh)^2} - 2f_1(x,t)h, \tag{B.18}$$

where $f_1(x,t)$ is defined by (B.14b).

Now that the velocity, u, is known, the integral term in the kinematic boundary condition, Eq. (B.10), can be found. Furthermore, the mass flux, j, is expressed by its dimensionless constitutive expression, Eq. (A.18). The result is the following interface equation:

$$h_t + \frac{EN}{1+Nh} + \frac{\partial}{\partial x}\int_0^h \left[f_1(x,t)z^2 + f_2(x,t)z\right]\mathrm{d}z = 0. \tag{B.19}$$

Substituting the explicit expressions from Eqs. (B.14b) and (B.18), for $f_1(x,t)$ and $f_2(x,t)$, in Eq. (B.19), gives the following interface equation:

$$h_t + \frac{EN}{1+Nh} + \frac{1}{C}\frac{\partial}{\partial x}\left\{\frac{h^3}{3}\left[h_{xxx}\left(1 - \frac{F}{1+Nh}\right) + \frac{FNh_{xx}h_x}{(1+Nh)^2} + \frac{2SN^3h_x}{(1+Nh)^3} - \frac{3\bar{A}Ch_x}{h^4}\right]r + \frac{FNh_xh^2}{2\theta_0^2(1+Nh)^2}\right\} = 0. \tag{B.20}$$

This is a highly non-linear and complex partial differential equation, which is difficult to solve, even numerically.

The temperature and velocity fields depend on the profile of the liquid–vapor interface, $h(x,t)$, and hence, unless it is known, they cannot be solved. The excessive complexity of Eq. (B.20) proved to be prohibitive, at this stage, for further use, and it was necessary to apply simplifying assumptions. To this end, the de Gennes hydrodynamic approach was incorporated in order to simplify the hydrodynamic treatment of the problem.

B.3. Analytical solution of the flow field

If the solution of Eq. (B.20) is known, the velocity field can be derived. The tangential velocity component, u, is given by Eqs. (B.14a) and (B.14b), and the normal velocity component, w, can be derived from continuity. Integrating the latter gives

$$\int (u_x + w_z)\,\mathrm{d}z = f_4(x,t), \tag{B.21}$$

where $f_4(x,t)$ is an integration constant. Hence

$$w(x,z,t) = f_4(x,t) - \int u_x\,\mathrm{d}z. \tag{B.22}$$

Substitution of u, from Eq. (B.14a), in (B.22), gives w as

$$w(x,z,t) = f_4(x,t) - \left[f_1(x,t)_x \frac{z^3}{3} + f_2(x,t)_x \frac{z^2}{2} \right]. \quad \text{(B.23)}$$

The no-penetration boundary condition of w at $z = 0$, Eq. (A.17), is used to determine the coefficient $f_4(x,t)$,

$$f_4(x,t) = 0. \quad \text{(B.24)}$$

In summary, the non-isothermal microscale temperature and flow fields can be solved analytically, provided that the profile of the liquid–vapor interface is solved first as a function of x and t.

References

[1] M. Ben David, Y. Zvirin, Y. Zimmels, Determination of the quench velocity and rewetting temperature of hot surfaces. Formulation of non-isothermal microscale hydrodynamic model, Phys. Rev. E. 59 (1999) 6687–6698.

[2] V.E.B. Dussan, On spreading of liquids on solid surfaces: static and dynamic contact angles, Ann. Rev. Fluid Mech. 11 (1979) 371–400.

[3] C. Huh, L.E. Scriven, Hydrodynamic model of steady movement of a solid/liquid/fluid contact angle, J. Colloid Interface Sci. 35 (1971) 85–101.

[4] V.E.B. Dussan, S.H. Davis, On the motion of a fluid–fluid interface along solid surface, J. Fluid Mech. 65 (1974) 71–95.

[5] L.H. Tanner, The spreading of silicone oil on horizontal surfaces, J. Phys. D: Appl. Phys. 12 (1979) 1473.

[6] J. Lopez, C. Miller, E. Ruckenstein, Spreading kinetics of liquid drops, J. Colloid Interface Sci. 56 (1976) 460–468.

[7] P.G. de Gennes, Wetting: statics and dynamics, Rev. Modern Phys. 57 (1985) 827–863.

[8] H.P. Greenspan, On motion of small viscous droplet that wets a surface, J. Fluid Mech. 84 (1978) 125–143.

[9] P. Ehrhard, S.H. Davis, Nonisothermal spreading of liquid drops on horizontal plants, J. Fluid Mech. 229 (1991) 365–388.

[10] R.L. Hoffman, A study of the advancing interface. I. Interface shape in liquid–gas systems, J. Colloid Interface Sci. 50 (1975) 228–241.

[11] P.G. de Gennes, X. Hua, P. Levinson, Dynamics of wetting: local contact angles, J. Fluid. Mech. 212 (1990) 55–63.

[12] S. Olek, Y. Zvirin, E. Elias, Rewetting of hot surfaces by falling liquids films as a conjugate heat transfer problem, Int. J. Multiphase Flow 14 (1988) 13–33.

[13] S. Olek, Y. Zvirin, E. Elias, The relation between rewetting temperature and the liquid–solid contact angle, Int. J. Heat Mass Transfer 31 (1988) 898–902.

[14] J.P. Burelbach, S.G. Bankoff, S.H. Davis, Nonlinear stability of evaporating/condensing liquid films, J. Fluid Mech. 195 (1988) 463–494.